AIAA

NAGW-122

WASHINGTON
UNIVERSITY
IN ST. LOUIS

McDonnell Center For the Space Sciences

SCINTILLATOR-FIBER CHARGED-PARTICLE TRACK-IMAGING DETECTOR

W. R. Binns, M. H. Israel, and J. Klarmann

Department of Physics and McDonnell Center for the Space Sciences

Washington University

St. Louis, Missouri 63130

Accepted for publication in Nuclear Instruments and Methods (1983).

ABSTRACT

A scintillator-fiber charged-particle track-imaging detector has been developed using a bundle of square cross section plastic scintillator fiber optics, proximity focused onto an image intensified Charge Injection Device (CID) camera. The tracks of charged particles penetrating into the scintillator fiber bundle are projected onto the CID camera and the imaging information is read out in video format. We have exposed our detector to beams of 15 MeV protons and relativistic Neon, Manganese, and Gold nuclei and have obtained images of their tracks. This paper presents details of the detector technique, properties of the tracks obtained, and preliminary range measurements of 15 MeV protons stopping in the fiber bundle.

I. INTRODUCTION

Many experiments require localization of charged particle tracks (e.g., for position of energy deposition, detector pathlength corrections, and particle trajectory determinations). With the advent of Charge Coupled and Charge Injected Device (CCD/CID) arrays it has become possible in principle to individually detect and analyze the light output from large numbers ($\sim 10^5$) of scintillation detectors at video rates. Also recent advances in fiber optic production techniques[1-2] have resulted in the development of scintillator fibers with much improved light piping characteristics over that of early efforts.[3-4] We have combined these two developments with image intensification techniques to develop an electronic charged particle track imaging detector which has imaged tracks to a resolution of $\sigma \approx 100$ μm.

Section II of this paper describes the detector concept including a description of the scintillator fiber physical characteristics and production technique, and the intensified camera system which detected light from the fibers. This is followed in section III by a discussion of light piping in a square cross section fiber for photons produced internal to the fiber. Measurements of light attenuation within fibers and charged particle track imaging are described in section IV followed by our conclusions in section V.

II. DETECTOR CONCEPT

A. Scintillator Fibers

The detector we have developed consists of a "bundle" of scintillator fibers proximity focused onto an image intensified CID video camera system. A charged particle penetrating into the bundle produces scintillation light in each fiber traversed, and a portion of the light is light piped along each stimulated fiber to the image intensifier (Figure 1). Thus a projection of the track is imaged onto the image intensifier face. This image is then intensified and projected onto the CID array from which the imaging information is read out in video format.

The scintillator fiber bundle consists of 2.7×10^3 individual fibers bonded together into a bundle with cross-sectional dimensions 0.9×1.2 cm^2 and length 40 cm. Individual fibers are square in cross-section, are nominally 200 μm on a side including a cladding wall thickness of about 14 μm, and are 40 cm in length. Figure 2 shows an end view of the bundle cross-section. A square cross-section was chosen for the fibers to eliminate holes and minimize non-scintillating material between fibers so that a more precise determination of the range of stopping charged particles might be obtained than would be possible for circular cross-section fibers. KSTI-415 plastic scintillator[5] which has a polystyrene base and peak fluorescence emission at 415 nm is used for the fiber core, and the cladding material is acrylic. The fibers were drawn from a square cross section acrylic tube (dimensions $3.3 \times 3.3 \times 34$ cm^3) filled with plastic scintillator. The scintillator had been previously ground up and extruded into the acrylic tube. A polystyrene based scintillator was chosen instead of the more usual polyvinyl toluene (PVT) based scintillator with the refractive index of polystyrene 1.62 (for λ = 436 nm) compared with 1.61 for PVT. Thus

a slightly larger fraction of the emitted light undergoes total internal reflection for a given cladding refractive index (for acrylic, n = 1.50). An additional advantage of the polystyrene based scintillator is that it is considerably less expensive than available PVT based scintillator.

Following the fiber drawing operation the fibers were grouped together and bonded into 40 cm long ribbons with cross sectional dimensions 0.02 x 1.2 cm and the ribbons were then stacked to form the 0.9 x 1.2 cm^2 cross section bundle. Thin coats of epoxy (Epotek 301) were used to form the fibers into ribbons and the ribbons into the bundle. The ends of the bundle were cut and polished to provide a flat surface for proximity focusing onto the face of an image intensified CID array camera system. Development and fabrication of the fibers and fiber bundles was carried out by "Fiber Optics Development Systems, Inc."[6]

B. Camera System

The camera system (ITT-F4144) was purchased from the Electro-Optical Products Division of ITT and is essentially an intensified General Electric TN-2500 CID video camera. The intensifier is a gateable, dual microchannel plate, 18 mm diameter image intensifier tube with a fiber-optic face plate and bi-alkali photocathode. The red phosphor output is fiber optically coupled to a CID array which is a silicon photodiode array of 244 x 248 pixels, each pixel having dimension of 36 μm x 46 μm. Since the scintillator fiber output is imaged onto the CID array with a magnification of 1, the output of a single fiber is imaged onto about 24 pixels. The CID array is read out through the Camera Control Unit (CCU) in standard analog video format (Figure 3). The analog output is recorded onto video tape using a Panasonic NV-8320 video recorder. The video recorder operating in its

"stop frame" mode is then played into an Apple II computer equipped with a Digisector card (Microworks DS-65) which allows an individual frame to be acquired by the Apple in 8 seconds and the intensity from each pixel to be digitized into 6 bits. This mode of data acquisition and analysis is advantageous in that large quantities of data can be acquired and analyzed easily but has the problem that intensities on a pixel by pixel basis are not precisely repeatable if one reanalyzes the same frame of information, presumably owing primarily to jitter in the magnetic head of the video recorder operating in the stop frame mode. This is not a serious problem for the experiment reported here since a single fiber is imaged onto about 24 pixels and the fluctuations in the sum of these pixel intensities are typically $\sigma \sim 9\%$. The CCU also provides a digital video output in an 8 bit/pixel parallel format which is clocked out at a word rate of 4.5 MHz.

For more precise data anlysis we have developed a Memory/CCU interface system which acquires one frame of data from the CCU 8 bit parallel digital output and stores it in a 64K byte static RAM. This information can then be transferred to the Apple II and recorded on disk for analysis.

The camera system can be operated in the usual continuous readout video mode but for transient events occurring on a time scale less than one frame time (33 m.s.) this often results in information being divided between two successive frames. To avoid this problem we operate the camera in the "staring" or "inject inhibit" mode. In this mode of operation the camera "stares" without being read out for a predetermined integral number of frame times. (For the data presented in this paper the staring time was 1 frame time or 33 m.s.) During this staring time the image intensifier is gated "on" so that light from any particle traversing the fiber bundle

will be detected. At the conclusion of this staring time the image intensifier is gated "off" to eliminate recording of "partial" events and the CID array is then read out into the static RAM and video recorder.

III. SQUARE FIBER LIGHT PIPING THEORY

We have calculated the fraction of light that will be light piped in a square cross section fiber for our case in which light is emitted isotropically internal to the fiber. For a photon emitted along a unit vector $\vec{r}$ (Figure 4) we write the vector in terms of its direction cosines as

$$\vec{r} = \sin\theta\cos\phi\,\vec{i} + \sin\theta\sin\phi\,\vec{j} + \cos\theta\,\vec{k} \quad .$$

This photon will be light piped down the entire length of the fiber (neglecting absorption) if the angles defined by $|\vec{r}\cdot\vec{i}|$ and $|\vec{r}\cdot\vec{k}|$ are both greater than the critical angle of reflection θ_c. ($\theta_c = \sin^{-1}(n_{clad}/n_{core})$ where n_{clad} and n_{core} are the refractive indices of the cladding and scintillator core material respectively. These angles are

$$\eta_{\vec{i}} = \cos^{-1}(\sin\theta\cos\phi) \geq \theta_c \quad ,$$

$$\eta_{\vec{k}} = \theta \geq \theta_c \quad .$$

It is irrelevant which reflection occurs first since the fiber walls are mutually orthogonal. Thus the fraction of photons light piped (L) along one direction of the fiber is the integral of the differential solid angle divided by 4π steradians with the limits of integration defined as above, i.e.,

$$L = \frac{\Omega}{4\pi} = \frac{4}{4\pi}\int_{\theta=\theta_c}^{\pi/2} \sin\theta\,d\theta \int_{\phi=\cos^{-1}\left(\frac{\cos\theta_c}{\sin\theta}\right)}^{\pi/2} d\phi$$

$$= \frac{1}{\pi}\left[\frac{\pi}{2}\cos\theta_c - \int_{\theta_c}^{\pi/2} \sin\theta\cos^{-1}\left(\frac{\cos\theta_c}{\sin\theta}\right)d\theta\right] \quad .$$

This integral has been evaluated numerically for the refractive index of the scintillator material (n_{core} = 1.62) and a cladding refractive index which is allowed to vary (Figure 5). For the acrylic cladding used on our fibers (n_{clad} = 1.50), 4.7% of the photons are light piped along each direction of the fiber. For comparison, L has also been calculated for circular fibers for the two cases a) where the emission is assumed to occur at the fiber center and b) where the emission is uniformly distributed along a line passing through the fiber axis. These are also plotted in Figure 5.

An interesting property of square cross section fibers which is a consequence of the requirements for TIR mentioned above is that L is independent of the position of light emission within the fiber. This is in contrast to circular fibers where L is a function of light emission position within the fibers and the variation in L is such that it increases as the particle "impact parameter" increases (the "impact parameter" is the perpendicular distance from the particle trajectory to the fiber center in units of the fiber radius). This increase together with the decreased pathlength of scintillator traversed as the impact parameter approaches unity results in a nearly constant <u>number</u> of photons being totally internally reflected (within ~1%) for impact parameters $\leq$ 0.9. However a significant fraction of light piped photons produced near the fiber edge are emitted with a large pitch angle relative to the fiber axis, resulting in a stronger attenuation for these "long pathlength" photons. Thus light emission from square fibers is inherently more uniform from fiber to fiber than for circular fibers.

IV. EXPERIMENT AND RESULTS

A. Attenuation Measurements

The scintillation light attenuation in the fiber bundle was measured by placing a ^{90}Sr electron source at various positions along the bundle and pulse height analyzing the light detected by the photomultiplier tube. Figure 6 shows a plot of the measured light intensity as a function of the ^{90}Sr source distance from the PMT tube face. For distance such that $7.5 \leq z \leq 32$ cm the data can be fit by an exponential $I = I_0 e^{-z/z_0}$ where $z_0 = 29.1$ cm. This slope is in excellent agreement with that obtained by Borenstein et al.[2] for 1 mm diameter circular cross-section fibers of NE110 with acrylic cladding (plotted as dashed line in Figure 6). The upturn in light intensity for distances less than 7.5 cm is an artifact of the experiment and is the result of scintillation light which is not light piped but is incident upon the end of the fiber bundle (and thus the photocathode). Borenstein et al.[2] find a break in the attenuation curve which occurs at a distance of about 32 cm. They attribute this break to a more rapid attenuation of the shorter wavelength photons than for longer wavelength photons, thus resulting in a flattening of the attenuation curve for distances greater than 32 cm. Our data point at z = 38 cm is consistent with this curve flattening but our estimated error bars are large enough so that additional data at greater distances would be necessary to confirm the change in slope.

To study the wavelength spectrum of light emerging from the fiber bundle as a function of light piping distance we have imaged the fiber bundle output face onto the entrance slit of a 0.3 m McPherson scanning

monochrometer. The monochrometer was fitted with a 1800 ℓ/mm diffraction grating and a 1 mm slit width was used. A 100 μCi ^{90}Sr source was placed at three different positions along the bundle. The light was detected by a Centronic 4292BA photomultiplier tube with a quartz faceplate. Figure 7 shows the wavelength spectrum obtained by scanning the monochrometer from 380 nm to 500 nm for the three light transmission distances. It is clear from the figure that the attenuation is stronger for the shorter wavelength photons than for longer wavelength photons and this results in an increasingly longer wavelength cutoff as the light piping distance becomes greater.

B. Track Imaging

To explore the capabilities of this technique for imaging charged particle tracks we have exposed our detector to beams of 15 MeV protons, and relativistic Neon, Manganese and Gold nuclei.

The Neon, Manganese, and Gold nuclei were obtained at the Lawrence Berkeley Laboratories Bevalac accelerator and had energies of 640, 1200, and 1000 MeV/amu respectively. Figures 8a and 8b show tracks of Ne and Au nuclei penetrating through the fiber bundle. We would expect the width of the Ne tracks to be about 200 μm (1 fiber dimension) since the tracks were directed into the fiber bundle perpendicular to the y-z plane (parallel to the ribbons). The track width intensity distribution is given in Figure 9 for a Neon track. The distribution is essentially gaussian with a full width half maximum of 230 μm, in good agreement with the fiber dimension. There are two sources of track broadening which are intrinsic to the camera system and not related to fiber size. The image intensifier is capable of resolving 18 line pairs/mm. Thus for a single photoelectron at the photocathode we expect a photon intensity distribution

at the CID array which has a σ of 24 μm. This distribution is roughly gaussian but with tails that are broader than for a gaussian. Thus for our present one-to-one magnification coupling between the image intensifier and the CID array, light from a single photoelectron is expected to be distributed over several adjacent pixels. Secondly the Modulation Transfer Function (MTF) for the CID array is 65% for the rows and 95% for the columns. The broadening of tracks from the intrinsic camera effects are small compared to the fiber size and so have little effect for the conditions of this experiment. If the fiber size projected onto the image intensifier becomes comparable to the size of an individual pixel however, these effects will be more significant. Thus the intrinsic positional resolution of this detector system would appear to be determined by the fiber dimensions although the resolution in pathlength actually obtained was dominated by inhomogeneities in the fiber bundle used in this test.

15 ± 1 MeV proton obtained from the Washington University Medical School Cyclotron were also directed into the fiber bundle parallel to the ribbons. Several of these tracks are shown in Figure 10. The range of a 15 MeV proton is 2.5 mm in polystyrene which corresponds to about 12 fibers. In addition to the fiber material itself, the epoxy used in the bundle construction was present in varying thicknesses on the particle entrance side resulting in a variation in track length. However no track length greater than 2.8 mm has been observed, which is consistent with the expected uncertainty in range determination due to the fiber dimensions and the beam energy uncertainty.

In order to obtain a pathlength distribution measurement, a second run was taken with 15 MeV protons incident perpendicular to the x-z plane (perpendicular to the plane of the ribbons). Figure 11 is a histogram of our track length measurements. We observe the peak of the track length distribution (solid line in figure) between 1.6 and 1.8 mm with a tail toward shorter track lengths. This peak track length is shorter than the 2.5 mm range of a 15 MeV proton owing to material penetrated by the proton beam before entering the fiber bundle. (Much of this material was not present for the conditions of the first run described above.) A microscopic examination of the fiber bundle proton entry side revealed an epoxy layer with thickness varying from about 100 to 300 μm with some localized "bumps" that were as much as 400-500 um thick. In an attempt to reduce the fluctuations in amount of epoxy traversed before the protons entered the fibers, a subset of these particles was selected such that their entry into the fibers was restricted to a 500 μm x 1 cm strip in the x, z plane. A histogram of these particles is plotted as a dashed line in Figure 11. This selection reduces the tail on the distribution although the particle statistics are low. In addition to this source of fluctuations in our track length measurements, those protons which penetrate only nonscintillating cladding material at the end of their range (14% of the protons) will have their track length shortened by 1 fiber thickness (200 μm). Thus the track length distribution is consistent with that expected given the construction of this fiber bundle.

V. DISCUSSION AND CONCLUSION

We have demonstrated that scintillator fiber bundles coupled to an intensified CID camera can be used to image the tracks of charged particles and to determine the range of stopping charged particles. The fiber bundles that have been developed can in principle be scaled up considerably in size to make a large geometrical factor range detector with a resolution of σ = 100 um.

The limitations of this technique for determining the range and trajectory of charged particles are associated primarily with fiber size, dimensional uniformity, and bundle homogeneity. We are currently working to produce a fiber bundle with more uniform fiber dimensions and a minimum of adhesive to reduce the uncertainty in range determination.

For applications in which the arrival direction of the particle is not known (e.g., cosmic ray nuclei track imaging) it is necessary to determine the z component of the trajectory. This can be done as a simple extension of the above technique by crossing fiber layers to make a hodoscope in the x,z plane above the range detector and coupling the fibers to an intensified CID array to obtain at least two x,z positions with a y separation adequate to obtain the desired trajectory resolution.

We believe that the essential techniques for making these range and trajectory measurements have been demonstrated in this experiment although additional experimental work is required to refine them and to adapt them to particular applications.

ACKNOWLEDGEMENTS

We thank J. C. Weintraub for assistance in programming and data analysis and K. A. Lynch for her work in deliniating the fiber light piping characteristics. We also thank W. V. Schempp of the Department of Earth and Planetary Sciences for performing the wavelength spectrum measurements. This work has been supported in part by NASA Grants NAGW-122 and NGR 26-008-001 and in part by the McDonnell Center for the Space Sciences.

REFERENCES

1. S. R. Borenstein, R. B. Palmer, and R. C. Strand, Physica Scripta 23, 550 (1981).

2. S. R. Borenstein and R. C. Strand, IEEE Trans. Nucl. Sci. 29, 402 (1982).

3. G. T. Reynolds and P. E. Condon, Rev. Sci. Instr. 28, 1098 (1957).

4. L. Reiffel and N. S. Kapany, Rev. Sci. Instr. 31, 1136 (1960).

5. M. Bourdinaud and J. C. Thevenin, Physica Scripta 23, 534 (1981); KSH Plastics, Geel, Belgium.

6. "Fiber Optics Development Systems, Inc.", 427 Olive Street, Santa Barbara, California 93101.

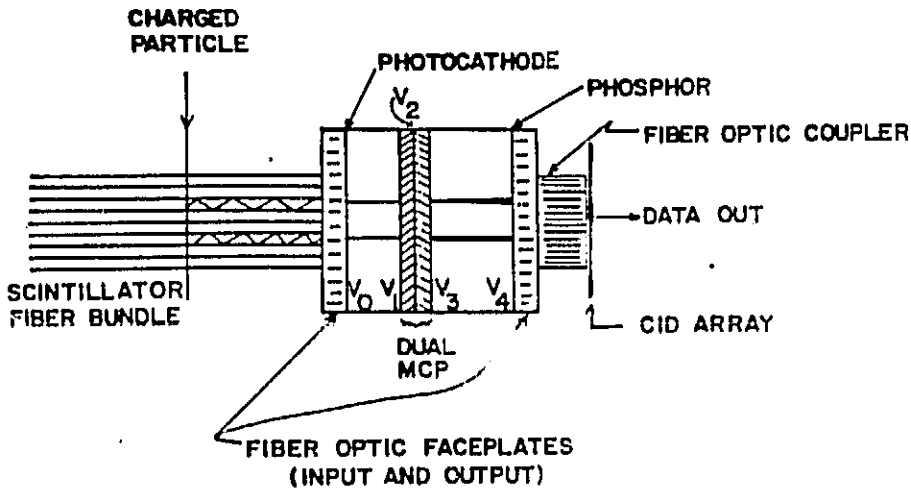

Figure 1. Schematic diagram of scintillator fibers proximity focused onto an image intensified CID array.

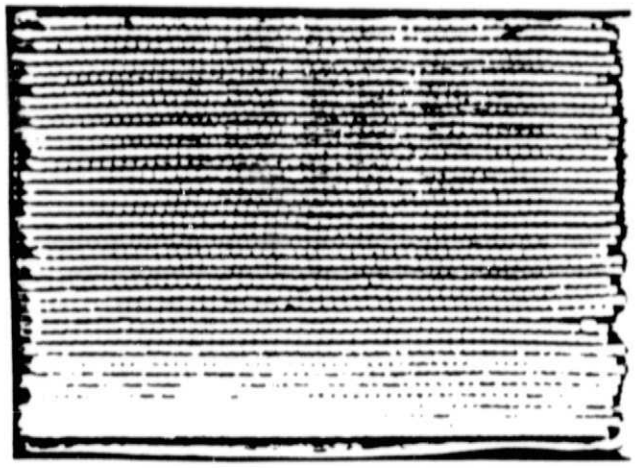

Figure 2. End view of scintillator fiber bundle.

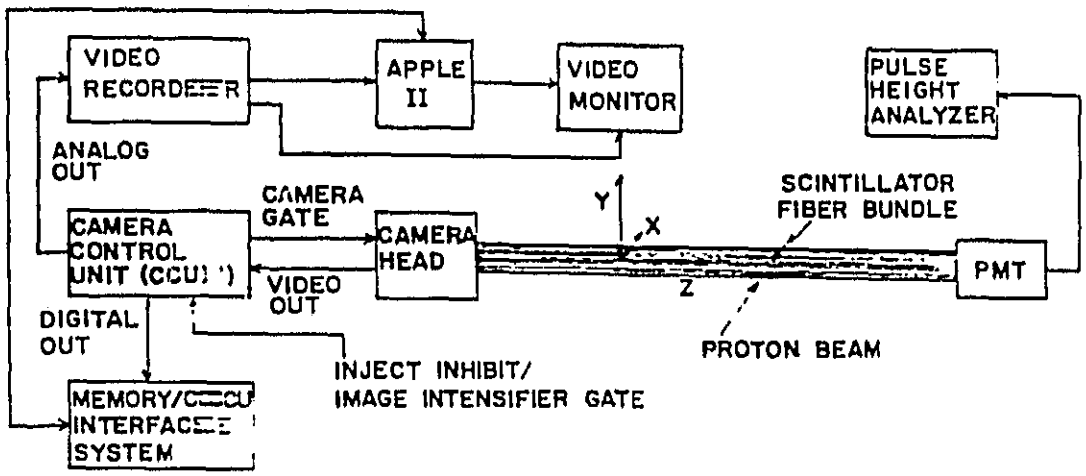

Figure 3. Experiment block diagram.

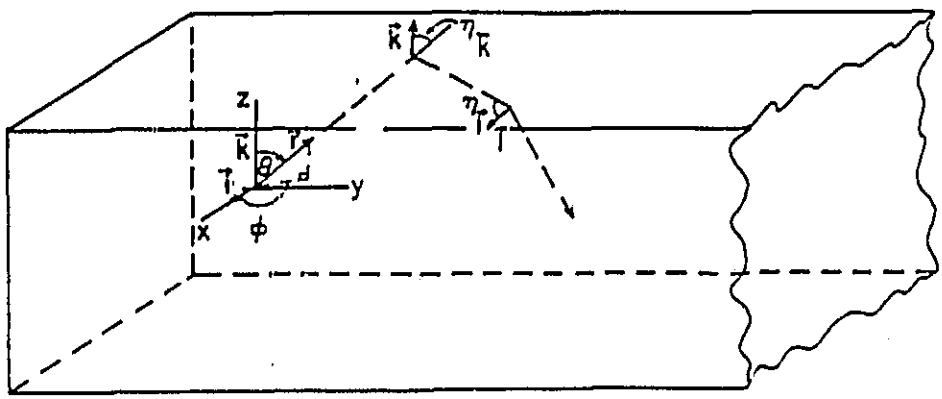

Figure 4. Coordinate system for square fiber light piping calculation.

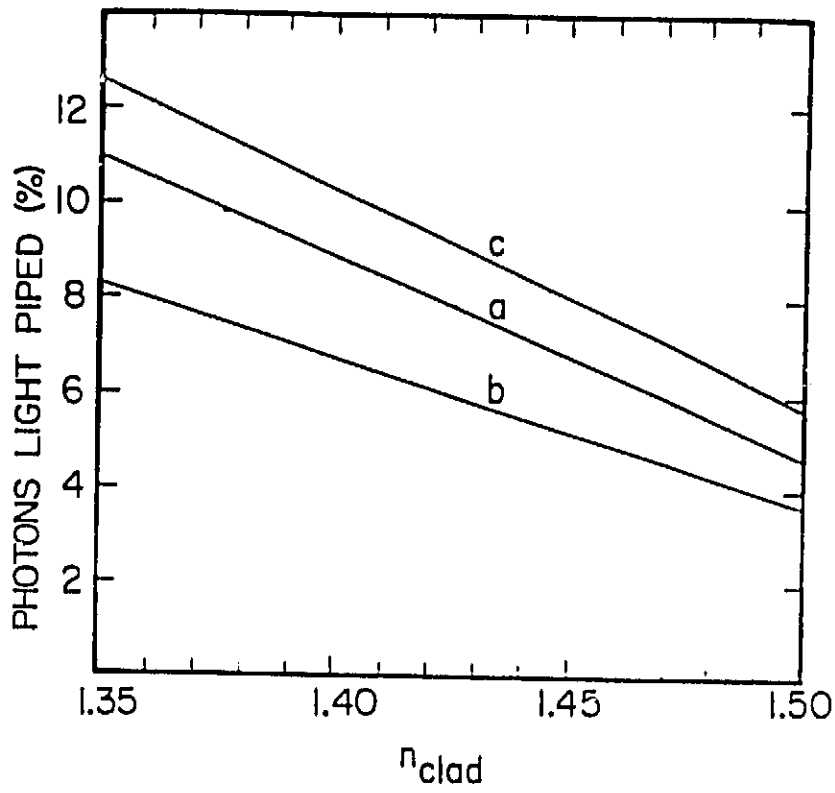

Figure 5. The fraction of scintillation photons emitted which are light piped along a fiber is plotted as a function of cladding refractive index for polystyrene core material (n = 1.62). Results are plotted for scintillation emission in a square cross section fiber (curve a), for a circular cross section fiber with light emission at the center of the fiber (curve b), and for a circular cross section fiber with emission uniformly distributed along a line passing through the fiber axis (curve c).

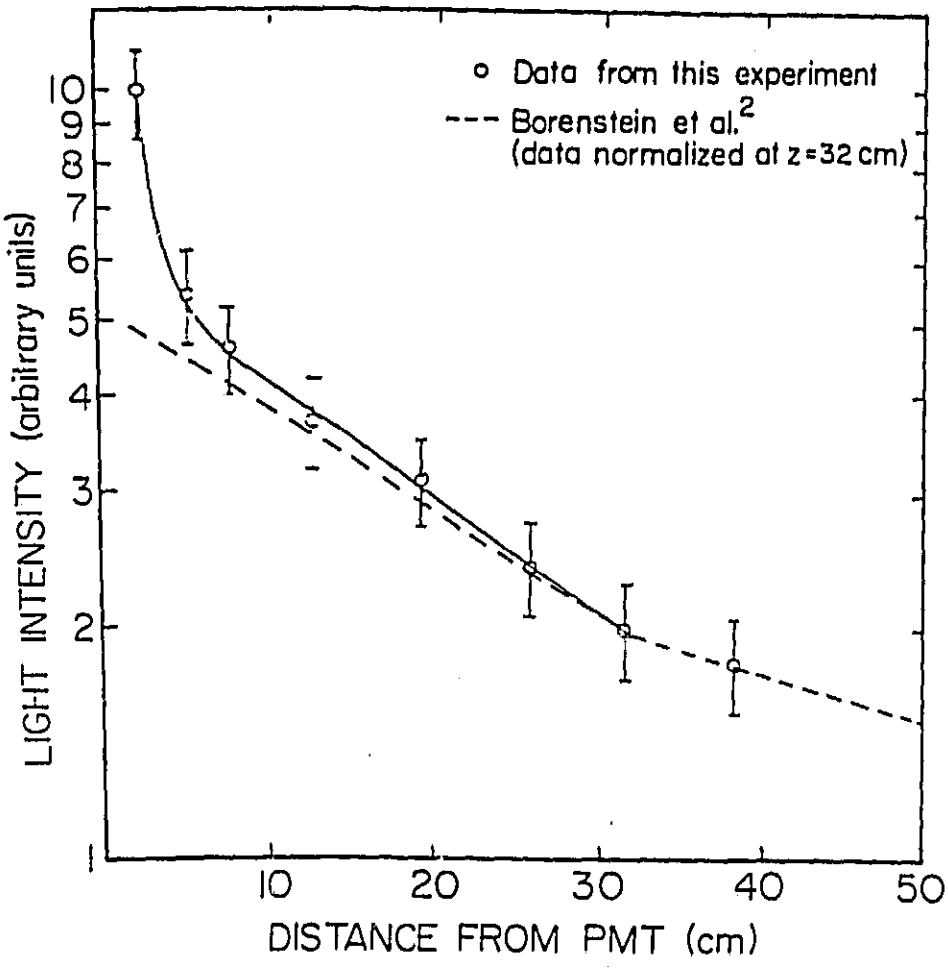

Figure 6. Attenuation of scintillation light as a function of light piping distance in scintillator fiber bundle.

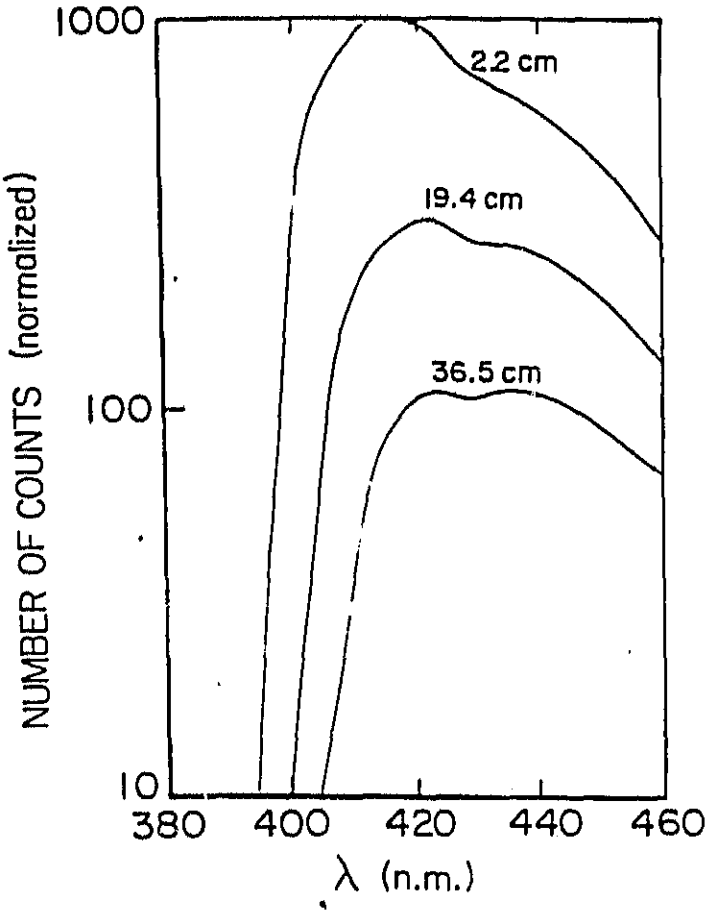

Figure 7. Wavelength spectrum of light emerging from scintillation fibers for several light piping distances.

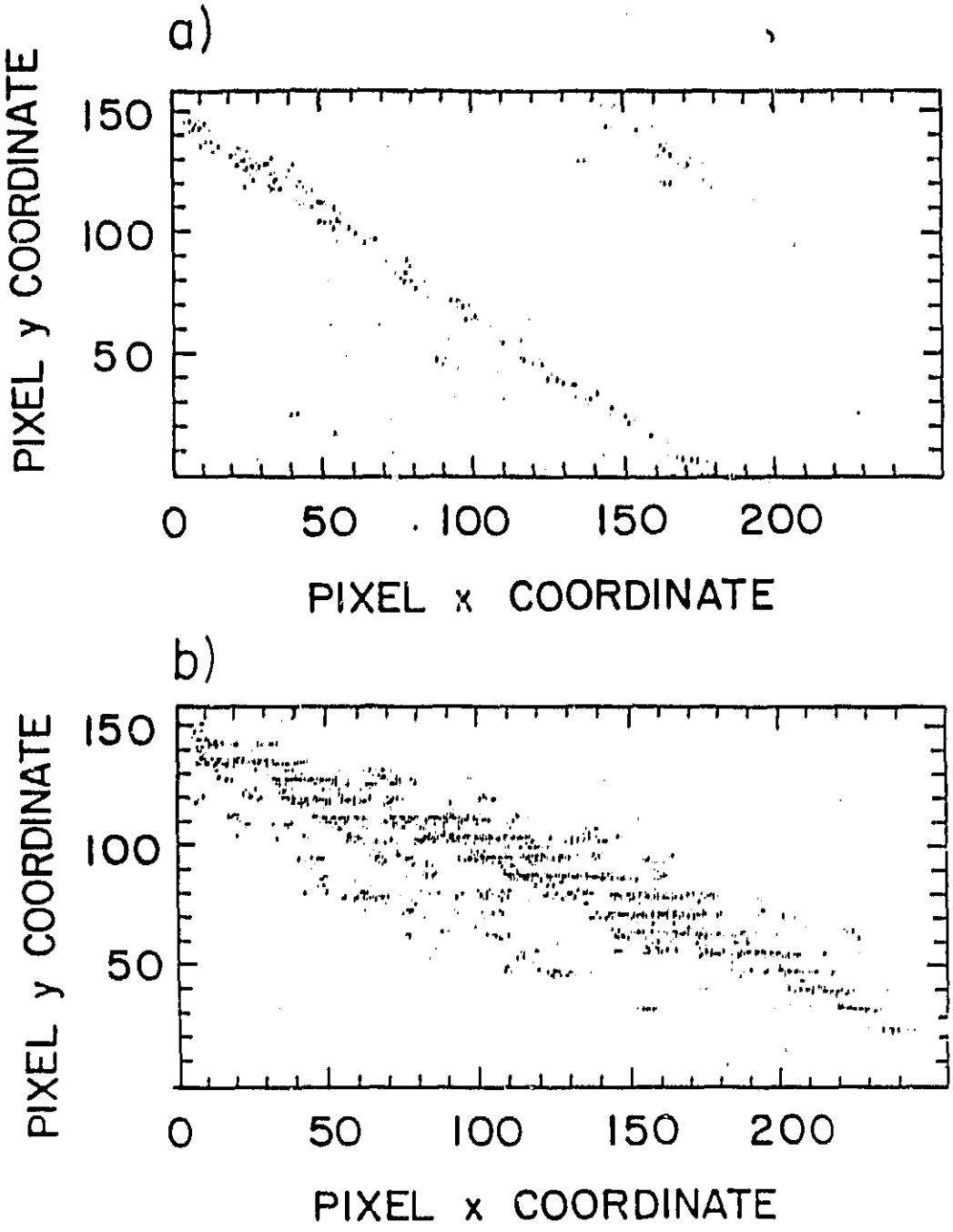

Figure 8. a) is the track of a Neon nucleus entering the fiber bundle at the lower right and penetrating through the bundle. The bundle is oriented so that the particle trajectory is parallel to the plane of the ribbons. The track in b) is that of a Gold nucleus with trajectory inclined to the plane of the ribbons by about 10°.

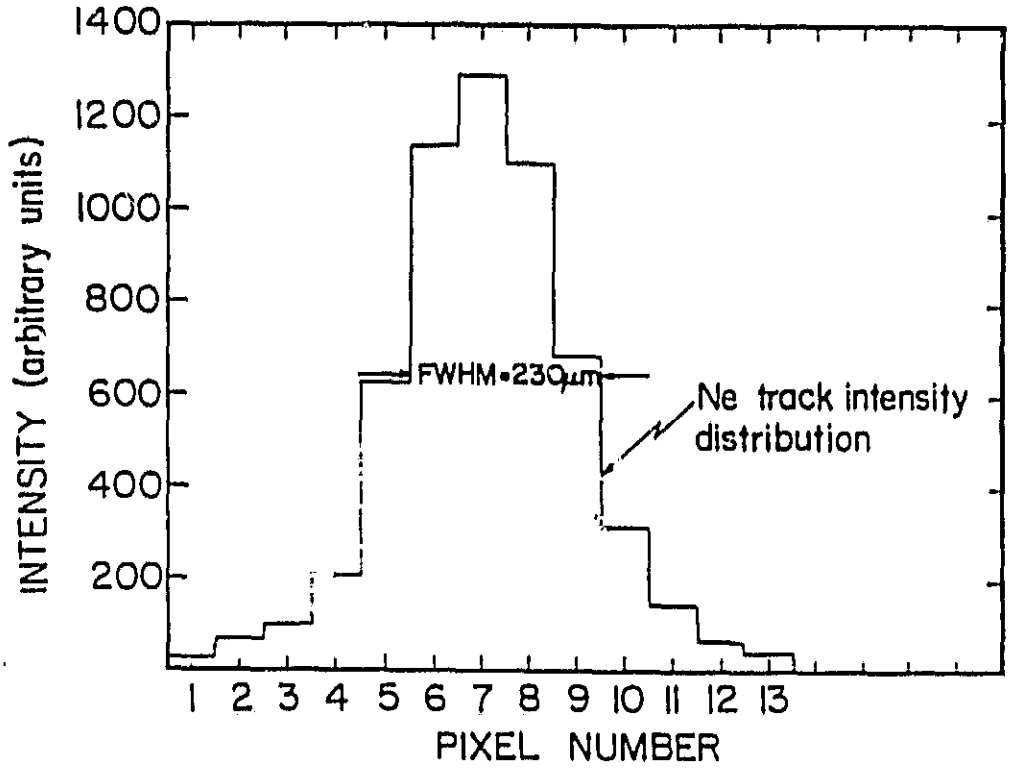

Figure 9. Neon track width intensity distribution.

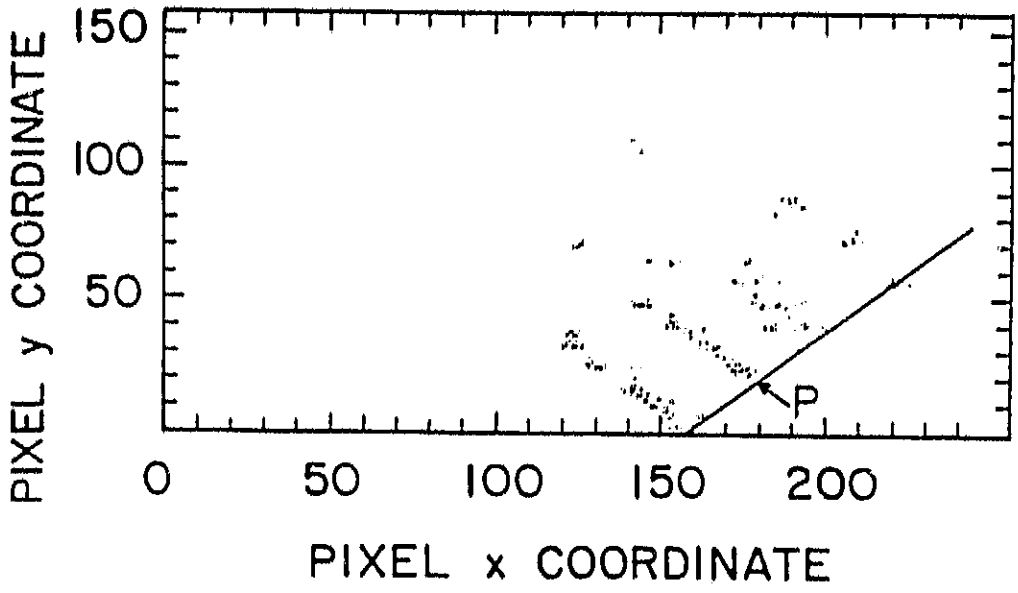

Figure 10. Tracks of 15 MeV protons. Protons entered from the lower right and stopped in the bundle. Their trajectory was in the plane of the ribbons. The angled line at the lower right is the approximate position of the bundle edge.

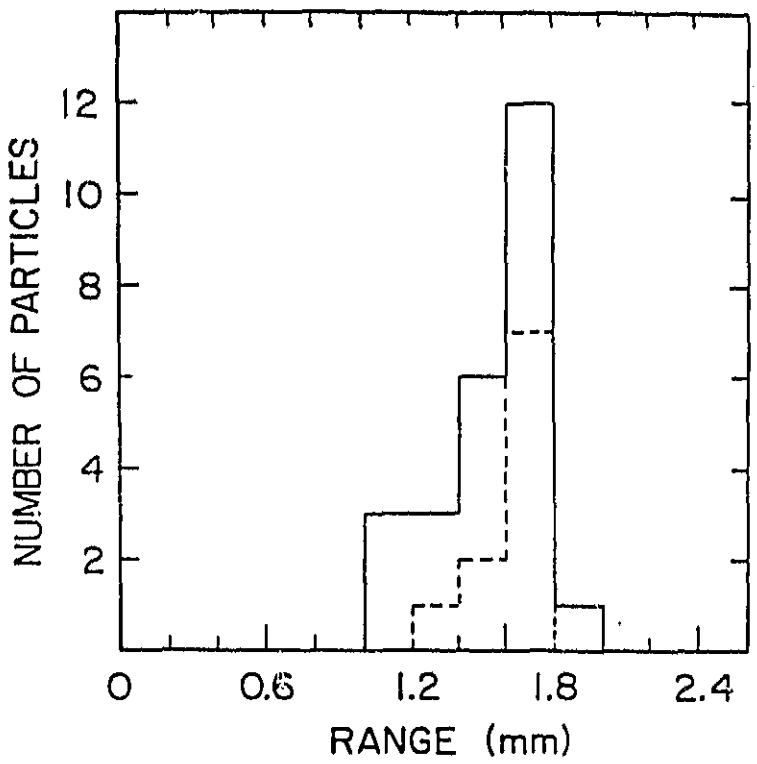

Figure 11. Track length distribution for 15 MeV protons in scintillator fiber bundle. Solid line—all particles studied. Dashed line—restricted particle entry region into bundle to reduce variation in material traversed before entering fiber bundle.